Please cite this paper as:
Rami A. Hawileh, Mohannad Z. Naser, Jamal A. Abdalla, Finite element simulation of reinforced concrete beams externally strengthened with short-length CFRP plates, Composites Part B: Engineering, Volume 45, Issue 1, February 2013, Pages 1722-1730, ISSN 1359-8368, https://doi.org/10.1016/j.compositesb.2012.09.032.

Finite Element Simulation of Reinforced Concrete Beams Externally Strengthened with Short-Length CFRP Plates

*Rami A. Hawileh[a], Mohannad Z. Naser[a] and Jamal A. Abdalla[a]

[a] *Department of Civil Engineering, American University of Sharjah, Sharjah P.O.Box 26666, UAE*
* *rhaweeleh@aus.edu*

ABSTRACT

Fibre Reinforced Polymer (FRP) materials have been recently used as novel materials to retrofit aging and deficient structures. Several research programs have succeeded in narrowing down the knowledge gap of the debonding mechanism associated with the failure of externally bonded FRP systems. This study seeks numerical investigation of plate debonding and performance of reinforced concrete (RC) beams externally strengthened with bonded Carbon Fiber Reinforced Polymers (CFRP) plates running for a length covering 25% of the shear span. The results are compared with plates covering 85% of the shear span in addition to a control unsrtrengthened specimen. The aim of this paper is to develop 3D finite element (FE) models that can accurately simulate the response and performance of RC beams externally strengthened with short-length CFRP plates. A total of six beams were modeled and the load-midspan deflection results and failure modes were compared with experimentally measured data published in the literature. Two out of the five strengthened beams were bonded to the soffit of the beams without any means of end anchorages. The other three beams were strengthened with CFRP plates and anchored transversely at the plate's ends with different arrangements of CFRP U-wrap sheets. The developed models incorporate the different material nonlinear constitutive laws including the bond-slip action between steel rebars and surrounding concrete and debonding at the CFRP-concrete interface. The predicted and measured load-midspan deflection response results in addition to the failure modes are compared. It was observed that the predicted FE results are in good agreement with the experimental measured test data. A parametric study was then performed using the validated FE model to investigate the effect of the flexural reinforcement bar diameter as well as arrangements of the CFRP U-wraps. It has been concluded that the developed FE models are capable of accurately predicting and capturing capacity the debonding failure mode of RC beams strengthened with FRP plates.

Keywords: A. Carbon fibre; B. Debonding; B. Interface/interphase; C. Finite element analysis (FEA)

1. INTRODUCTION

The use of externally bonded strengthening carbon fiber reinforced polymer (CFRP) systems in retrofitting and strengthening of reinforced structural members in shear and flexure has gained a wide acceptance in the rehabilitation engineering community [1-8]. The CFRP composite materials are known of their superior mechanical properties in-terms of high strength to weight ratio, resistance to corrosion, thermal resistance, and ease of installation. Several experimental studies have shown the effectiveness of using externally bonded CFRP composites to improve the flexural capacity of RC beams [9-15]. However, most of the previous studies were conducted using FRP plates or sheets externally attached to the soffit of RC beams running along the full span length. The effect of having shorter FRP plate lengths did not receive similar attention. It has been observed that the open literature and design codes lack [15-18] information on the behavior of RC beams strength with short-length CFRP plates.

Please cite this paper as:
Rami A. Hawileh, Mohannad Z. Naser, Jamal A. Abdalla, Finite element simulation of reinforced concrete beams externally strengthened with short-length CFRP plates, Composites Part B: Engineering, Volume 45, Issue 1, February 2013, Pages 1722-1730, ISSN 1359-8368, https://doi.org/10.1016/j.compositesb.2012.09.032.

One of the few experimental studies that considered the effects of using short length CFRP plates was conducted by Al-Tamimi et al. [15]. Al-Tamimi et al. [15] investigated experimentally the effect of strengthening RC beams in flexure with short-length CFRP plates with different anchorage systems. The test parameters included the CFRP plate length/shear span ratio, different end plate anchorage systems and the implementation of single layer of U-wrap sheet as opposed to two layers of U-wrap sheets with perpendicular fiber orientation. The results of the strengthened specimens were compared with an unstrengthened specimen and a control strengthened specimen with a CFRP plate running for 85% of the shear span. Results for the load-midspan deflection response of the tested specimens along with the associated failure modes were presented [15]. It was concluded that the reduction in the CFRP plate length will result in a reduction in the overall cost of the CFRP strengthening alternative. In addition, the load carrying capacity of the beam specimens could be significantly improved with shorter length CFRP plates if such strengthened beams are properly anchored with CFRP U-wraps mounted at the ends.

Several numerical programs have studied the performance of strengthened RC members by means of finite element (FE) simulation [19-24]. Lu et al. [19] developed a meso-scale FE model to predict the debonding process in FRP-concrete bonded joints using a fixed angle crack model employed in a very fine mesh size and the results showed good correlation with measured experimental data. However, this model was used to simulate bonded concrete joints (prisms) and was not tested against full scale RC members. In addition, the use of very fine mesh sizes would increase the computational time and complicate the solution processes.

Hawileh [20] developed a 3D nonlinear FE model that uses springs and cohesive elements to predict the debonding phenomenon of different NSM strengthening systems. Spring elements were used to model the bond-slip action between the steel reinforcement and the surrounding concrete and between the FRP NSM bars and the surrounding resin or mortar surfaces. In another study, Hawileh et al. [21] developed a FE model that was able to capture the response of deep beams with openings strengthened with externally-bonded CFRP sheets. The authors used cohesion elements along with a bond-slip model to simulate the bond between the CFRP sheets and adjacent concrete surfaces. It was concluded that the use of cohesive elements can accurately predict the response and failure mode of the strengthened specimens. Similarly, Chen et al. [22] investigated the effects of various modeling assumptions on the interfaces between concrete, main steel bars and shear stirrups, as well as between concrete and FRP on the shear performance of strengthened RC beams. Interfacial elements were used to model the bond between internal steel reinforcement (flexure bars and stirrups) and concrete as well as between the FRP and concrete interfaces. Chen et al. [22] reported the importance of modeling the bond behavior between steel reinforcement, concrete and FRP in achieving good correlation with the measured experimental results.

The aim of this paper is to numerically predict the performance of RC beams strengthened with short-length CFRP plate running for 25% of the shear span length with and without end anchorages. Three-Dimensional nonlinear finite element (FE) models were developed using the finite element simulation code, ANSYS [23]. The model considers the different material constitutive laws for concrete in tension (cracking) and compression, steel yielding, and the CFRP orthotropic material properties. In addition, the bond-slip action between the steel bars and surrounding concrete surfaces, and bond between the CFRP plate and adjacent concrete interfaces is considered in the developed FE models, presented herein. For the specimens anchored at both ends with U-Wrap CFRP sheets, cohesion elements are used at the interface between the CFRP sheets and concrete surfaces to simulate the bond between them. The models are validated by comparing the predicted load-deflection response, ultimate load capacity and failure modes with the measured experimental data conducted by Al-Tamimi et al. [15]. Based on the good agreement between the experimental and FE results, a parametric study was designed and performed. The parametric study varied the size of the tension reinforcement as well as arrangements of the CFRP U-wraps. The FE modeling of such a problem, if simulated properly, could serve as a numerical platform for predicting the behavior and capturing the response of RC beams externally strengthened in flexure with short-length CFRP laminates and anchorage systems.

2. FINITE ELEMENT MODEL DEVELOPMENT

2.1. Geometry of the developed FE models

In this study, six 3D FE models were developed using the simulation environment, ANSYS 11.0 [23]. The developed FE models are based on the specimens tested in the experimental program of Al-Tamimi et al. [15]. Table 1 shows the experimental test matrix along with the numerical designation of the specimens used herein.

The tested RC beams are 1840 mm long, 180 mm deep and 110 mm wide. The clear span of the tested RC beams is 1690 mm. In addition, the RC beams were heavily reinforced in shear by closely spaced internal steel stirrups to force flexural failure. Figure 1 shows the detailing and loading set-up of the tested RC beams. It should be noted that all specimens were tested in four-point bending set-up. The loading was increased incrementally until failure. Further, the two loading points are equally spaced 238.5 mm from the beam’s mid-span. The shear span of the beam specimens is 561.5 mm. The main flexural steel reinforcement are two 10 mm diameter BS B500B (BS4449) bars located at a depth of 155 mm from the compression fibers of the beam. In addition, two 10 mm bars were included in the compression zone at a depth of 25 mm from the aforementioned location. The shear reinforcement consisted of 8 mm diameter mild steel bars spaced at 80 mm center to center.

The first specimen designated as “CB” was unstrengthened to serve as a control specimen. The second and third beam specimens (B90P, B50P) are strengthened with CFRP plates without end anchorages, running symmetrically about the midspan of the beam specimens for a total length of 1521 and 845 mm, respectively. The CFRP plate thus covered 85% and 25% of the shear span for B90P and B50P specimens, respectively. Specimen "B50PW" was similar to B50P but with one layer of transverse unidirectional 200 mm wide CFRP sheets U-wrapped at plate ends and mid-span. Specimen B50PWD was strengthened and anchored in a similar fashion to B50PW, but with two layers of unidirectional U-wrapped CFRP sheets. The CFRP fiber directions in the two layers of sheets were perpendicular to each other. Finally, specimen B50PW1 is similar to B50PW but anchored with one layer of 400 mm wide CFRP U-wrap to investigate the effect of the width of the end CFRP wrap anchorage system. In order to distinguish between the experimental specimens and numerical models, the prefix “FE” is added to the labeling of the FE models.

Due to the symmetry of the geometry, loading, boundary conditions, and material properties, a quarter FE model was built and simulated in the finite element software, ANSYS [23]. The advantage of building quarter models for the tested beam specimens is the reduction in the total number of elements which will result in tremendous savings of computational time.

Figure 2 shows the developed FE models of the strengthened specimens. Figure 2a shows the boundary conditions and loading set-up. Figure 2 shows two planes of symmetry in the longitudinal and transverse directions of the all beam specimens. The symmetrical boundary conditions were developed by inserting vertical restrains (rollers) at each node located in the two planes of symmetry in the transverse and longitudinal directions.

2.2. Elements Description

Multiple element types were used to model this structure. The concrete material was modeled using SOLID65 brick elements [23]. The SOLID65 element has 8 nodes located at its corners. Each node has three translational degrees of freedom (d.o.f) in the x, y, and z directions. SOLID65 is capable of modeling both cracking and crushing of the concrete material. On the other hand, the main tension steel reinforcement are modeled using LINK8 [23] elements. LINK8 is a 3D spar (bar) element defined by two nodes with three translational degrees of freedom at each node. The element is capable of elastic-plastic deformation, stress stiffening, and large deformation. The CFRP plate is modeled using SHELL99 [23] elements with orthotropic material properties that have its own coordinate system, where the x-axis is in the direction parallel to the main CFRP fibers. An epoxy layer having a thickness of 1 mm was used to simulate the adhesive bond layer at the CFRP to concrete interface using SOLID45 elements [23]. Solid45 [23] is a brick element similar to SOLID65 but doesn’t have the capability of cracking in tension and crushing in compression. The rigid loading and vertical restrains supports are also modeled using SOLID45 [23] as shown in Fig. 2 with elastic steel material properties. Such modeling technique would prevent any major stress concentration on the concrete material at the specified concentrated loading locations.

This is a preprint draft. The published article can be found at:
http://www.sciencedirect.com/science/article/pii/S135983681200580X

Please cite this paper as:
Rami A. Hawileh, Mohannad Z. Naser, Jamal A. Abdalla, Finite element simulation of reinforced concrete beams externally strengthened with short-length CFRP plates, Composites Part B: Engineering, Volume 45, Issue 1, February 2013, Pages 1722-1730, ISSN 1359-8368, https://doi.org/10.1016/j.compositesb.2012.09.032.

In earlier numerical studies, the use of perfect bond between the concrete and steel reinforcement and between the CFRP plate and adjacent concrete was assumed [8, 24]. In this study, the bond-slip behavior between the concrete material and steel bars as well as the bond between the CFRP plate and adjacent concrete surfaces is simulated. The bond-slip between the steel reinforcement and concrete was modeled using COMBIN14 [23] spring elements. COMBIN14 has longitudinal capabilities in 1-D, 2-D, or 3-D applications. The longitudinal spring-damper is a uniaxial tension-compression element with up to three degrees of freedom at each node: translations in the nodal x, y, and z directions [23]. On the other hand, the bond behavior between the CFRP plate and adjacent concrete surfaces was simulated using INTER205 [23] cohesive elements. INTER205 is a 3-D 8-node linear interface element that is capable of simulating different interfaces between two surfaces as well as delamination process. The debonding occurs when initially coincident nodes experience increasing displacement (either longitudinally or transversely). INTER205 is defined by eight nodes each having three degrees of freedom.

2.3. Material Properties

The developed model comprise of several materials. Constitutive material laws are assigned to the different material components of the structure. The used concrete material had a compressive strength of 54 MPa. In addition, it had a modulus of elasticity of and Poisson’s ratio of the concrete material of 34.5 GPa, and 0.2, respectively. The compressive nonlinear concrete material is modeled using Hognestad et al. [25] model presented in Eq. (1).

$$f_c = f'_c\left[2\left(\frac{\varepsilon}{\varepsilon_o}\right)-\left(\frac{\varepsilon}{\varepsilon_o}\right)^2\right] \tag{1}$$

where,

f'_c is the stress in the concrete (MPa) corresponding to the specified strain, ϵ, and f'_c is the concrete ultimate compressive stress (MPa) and ϵ_o is the compressive strain corresponding to f'_c.

The concrete tensile stress-strain response is modeled using a linear elastic behavior up to the tensile rupture strength (f'_c). The tensile rupture strength is taken as $0.62\sqrt{f'_c}$ where f'_c is the compressive strength of concrete. Once the peak tensile stress is reached, the concrete tensile stress relaxation behavior is accounted for with a sudden drop in the concrete tensile strength equals to 0.6 f_r [23]. Then, a linearly descending tensile stress-strain curve (up to zero stress at a strain of 6 ε_t) is used, the ε_t is the concrete strain corresponding to f_r..

The steel reinforcement was assumed to follow an elasto-plastic behavior. The measured elastic modulus and yield strength of the main steel reinforcement is 202 GPa and 611 MPa, respectively. In addition, the used Poisson's ratio in the numerical simulation is 0.3.

The CFRP plate has a thickness and width of 1.4 mm and 100 mm, respectively. In addition, the CFRP plate has a tensile strength, modulus of elasticity and strain at rupture of 2800 MPa, 160 GPa and 1.69%, respectively. The elastic orthotropic material properties for the CFRP plate are taken as: E_x = 160 GPa, $E_{y,z}$= 16 GPa, $\nu_{xy,xz}$ = 0.28, ν_{yz} = 0.42, and $G_{xy,xz,yz}$ = 7 GPa. The CFRP plate was bonded to the concrete surfaces using Sikadur 30 LP adhesive. The mechanical properties of the Sikadur 30 LP are 10 GPa and 30 MPa for both, the modulus of elasticity and tensile strength, respectively. An assumed layer of Sikadur 30 LP having a thickness of 1 mm was used to simulate the bond layer at the CFRP -concrete interface.

2.4. Bond-Slip Model

Two bond-slip models were used in the presented FE models [20-21, 24]. The first model is used to simulate the bond action between the steel reinforcement and surrounding concrete material while the second model is used to simulate the interfacial bond relationships between the CFRP plate/sheet and concrete surfaces.

The bond-slip between the steel reinforcement and concrete is presented by Eq. (2). Equation 2 is based on the CEB-FIP model [26]:

$$\tau = \tau_u \left(\frac{s}{s_u} \right)^{0.4} \tag{2}$$

where,

τ is the bond stress at a given slip (s) in (MPa),

τ_u the maximum bond stress in (MPa),

s is the relative slip at a given shear stress in (mm),

s_u is the ultimate slip at τ_u in (mm),

The values of the maximum bond stress and slip depend on rebar type and surrounding materials. According to the CEP model [26], the values of $\sqrt{f_c'}$ and 0.6 mm were taken to simulate the τ_u and s_u, respectively.

The longitudinal bond-slip is implemented using the COMBIN14 [23] elements. COMBIN14 elements require a value for the longitudinal stiffness (k of the spring element which could be obtained from the secant of Eq. (2) as derived by Nie et al. [27] and presented in Eq. (3).

$$k = \frac{\pi}{s_u} p d_r N_r \tau_u \left(\frac{L_1 + L_2}{2} \right) \tag{3}$$

where,

p is the horizontal distance between the tension steel reinforcement bars in (mm), d_r is the diameter of the steel bars in (mm), N_r is the number of reinforcing bars and L_1 and L_2 represent the lengths of two adjacent reinforcement elements (LINK8) in (mm).

The second bond-slip model uses interface elements (INTER205) to simulate the debonding phenomena at the CFRP-concrete interface. The interface elements are placed along the longitudinal direction of the beam specimens at the surface of the epoxy layer. The implemented interface elements use the exponential form of the cohesive zone model developed by Xu and Needleman [28]. The developed exponential cohesive zone material model starts with an increasing segment up to the ultimate shear stress (τ_u) and its corresponding slip (s_u) and then proceeds with a softening response up to the ultimate attained slip which is assumed to equal to $4\times s_u$. The value of τ_u for each model is obtained using Eq. (4) which is proposed by Nabaka et al. [29] model:

$$\tau = \tau_{\max}\left(\frac{s}{s_0}\right)\left[3/\left(2+\left(\frac{s}{s_0}\right)^3\right)\right] \tag{4}$$

where, $\tau_{\max} = 3.5 f_c'^{0.19}$

$s_0 = 0.065\,\mathrm{mm}$

s is the slip between the concrete and CFRP interfaces

2.5. Failure Criteria

Failure is assumed to occur according to the following criteria:

1. For the unstrengthened beam specimen, failure is defined by yielding of the steel reinforcement in tension followed by concrete crushing. Concrete fails in compression when strain in the top compression fiber exceeds 0.003.

2. For the strengthened beam specimens with CFRP plates, failure is initiated by debonding of the CFRP plate from the soffit of the RC beam specimen.

It was attributed to the material nonlinearity, bond-slip action, debonding and associated large deformations that convergence of the solution was initially hard to achieve using the program default force convergence value of 0.005 [23]. Hence, failure of numerical simulation was assumed to occur when the solution of a 10 N load increment does not converge. In order to obtain convergence of the equilibrium iterations, the force convergence tolerance limit value was increased to 0.1. Typical used convergence tolerance limit range in concrete modeling is 0.05 to 0.2 [30].

3. RESULTS AND DISSCUSION

The validation of the FE models was conducted by comparing the predicted load-midspan deflection response and ultimate load capacity with that of the measured experimental data for the tested beam specimens. Table 2 shows a comparison between the predicted numerical and measured experimental load carrying capacity and corresponding deflection of the tested beam specimens. Furthermore, Figures 3-5 show the predicted and measured load-midspan deflection response of the tested and simulated beam specimens.

It is clear from Figures 3-5 and Table 2 that there is a good agreement between the experimentally measured and FE predicted load-midspan deflection results at all stages of loading till failure of the specimens. In addition, the difference between the predicted and measured load carrying capacity and ultimate deflection for the tested specimens is less than 5%. To further validate the FE models, the failure modes of the tested specimens were compared with those obtained numerically. Figure 6 shows a comparison between the simulated and experimental failure modes of the tested beam specimens. It is clear from the simulated and experimental results that the strengthened beams without end anchorage failed by plate debonding as shown in Fig. 6 (a), and the other strengthened beams with different U-wrap end anchorage systems failed by concrete cover delamination in the maximum moment region.

Thus, it could be concluded that the developed FE models are valid and reliable and could be used as a valid numerical tool to investigate the performance of RC beams strengthened with short-length CFRP plates with or without U-wrap anchorage systems.

4. PARAMETRIC STUDY

A parametric study is carried out in this section by developing thirteen additional models to investigate the effect of the flexural reinforcement ratio (bar diameter) and arrangements of the CFRP U-wraps of the beams strengthened with short-length CFRP plates. It should be noted that the FE models used in the parametric study have the same material constitutive laws and assumptions described earlier in the preceding sections.

4.1 <u>Effect of bar size of the steel tensile reinforcement</u>

Three additional FE models are developed for every strengthened case. The bar diameter for each additional model was 12, 16 and 20 mm, respectively. The designation of the new models is shown in Table 3 and included the diameter size as a suffix to the original designation of the original cases. Figures 7-10 show the effect of changing the bar size on the overall behavior of the different strengthened beams specimens. Table 3 summaries the results of the simulated specimens in terms of the predicted failure load and associated midspan deflection.

It is clear from Figs. 7-10 that increasing the bar size tend to increase the overall capacity of the beam specimens. On the other hand, the deflection response did not follow a certain trend. It was found that the deflection response is directly associated with the failure mode of the specimens. The failure mode of the different specimens varied according to the original strengthening configuration and steel reinforcement bar size.

Figure 7 shows that the failure mode of FE-B50P-12mm starts with yielding of the steel reinforcement followed by a sudden debonding of the CFRP plate and crushing of concrete. On the other hand, specimens FE-B50P-16mm and FE-B50P-20mm failed only via debonding of the CFRP plate. Specimens FE-B50PW-12mm, FE-B50PW-16mm and FE-B50PW-20mm shown in Fig. 8 failed in a similar manner to the specimens shown in Fig.7 except that crushing of concrete in specimen FE-B50PW-12mm was located at minor locations at the beam mid-span section.

Figure 9 shows that FE-B50PW1-12mm and FE-B50PW1-16mm failed by yielding of the tensile steel reinforcement and debonding of the CFRP plates while specimen FE-B50PW1-20mm failed by debonding of the CFRP plate. Finally, the mode of failure for specimen FE-B50PWD-12mm was yielding of the steel reinforcement followed by debonding of CFRP plate and crushing of concrete. On the other hand, FE-B50PWD-16mm and FE-B50PWD-20mm failed by debonding of the CFRP late prior to the yielding of the steel reinforcement.

4.2 Effect of arrangement of the CFRP U-Wrap

Based on the results of the previous parametric study section, a new model FE-B50PWD1 was developed. FE-B50PWD1 is a hybrid combination of FE-B50PW1 and FE-B50PWD models. The developed model has similar features to the FE-B50PW1 and FE-B50WD in which the CFRP fibers of the U-wraps are aligned in two perpendicular directions and the sheet had a width of 400 mm. Figure 11 shows the effect of the new anchorage system response and compared to that of FE-B50PW1 and FE-B50PWD models, respectively.

It is clear from Fig. 11 that using a wider CFRP U-wraps with two layers in which the CFRP fibers are aligned perpendicular to each other tends to enhance the beam's ductility when compared to the strengthened FE-B50PWA and FE-B50PWD beam specimens, mainly by delaying debonding of the CFRP plate. However, no obvious increase in the ultimate load capacity is observed.

5. SUMMARY AND CONCLUSIONS

Nineteen 3D nonlinear FE models were developed to simulate the response of RC beams strengthened in flexure with short-length CFRP plates herein. Six FE models were validated against the experimentally measured data in [15]. In addition, a parametric study consisting of thirteen models was conducted. The parametric study varied the size of the tensile steel reinforcement as well as the arrangement and width of the CFRP U-wrap anchorage sheet. Based on the results of this study, the following conclusions could be drawn:

- Good agreement between the measured experimental data and predicted FE models is observed at all stages of loading till failure.

- The overall comparison between the ultimate load carrying capacity and mid-span deflection at failure showed good agreement between the predicted FE values and the experimentally measured ones.

- The diameter of the flexural steel reinforcement (reinforcement ratio) contributes to the failure mode of the strengthened specimens. In general, the ductility of the beam will be reduced as the bar diameter increases leading to sudden brittle plate debonding failure mode.

- In general, the use of CFRP U-wraps tends to increase the overall capacity by delaying debonding of the CFRP plate.

- The use of an anchoring U-wrap system of two sheets aligned perpendicular to each other with a width of 400 mm seems to be an optimal anchorage configuration since it enhances the ductility of the strengthened beams by offering a wider bonded area. However, they do not tend to increase the overall flexural capacity of the strengthened beams.

The developed FE models presented in this study could serve as a numerical platform to the expensive and time consuming experimental testing. The developed FE models can be used to further to explore the behavior and predict the performance of RC beams externally strengthened in flexure with CFRP plates with different lengths and anchorage systems.

REFERENCES

1. N. Pešić, K. Pilakoutas. Concrete beams with externally bonded flexural FRP-reinforcement: analytical investigation of debonding failure. Composites: Part B, 43 (3) (2012), pp. 327-338.
2. V. Ramana, T. Kant, S. Morton, P. Dutta, A. Mukherjee, Y. Desai. Behavior of CFRP strengthened reinforced concrete beams with varying degrees of strengthening. Compos Part B: Engng, 31 (6/7) (2000), pp. 461–470.
3. M. Naser, R. Hawileh, J. Abdalla, A. Al-Tamimi. Bond Behavior of CFRP Cured Laminates: Experimental and Numerical Investigation. Journal of Engineering Materials and Technology, ASME, 134 (2012), pp. 1-9..

4. D. Kachlakev, D. McCurry. Behavior of full-scale reinforced concrete beams retrofitted for shear and flexural with FRP laminates. Composites: Part B, 31 (6/7) (2000), pp. 445-452.
5. A. Bilotta, M. Ludovico, E. Nigro. FRP-to-concrete interface debonding: Experimental calibration of a capacity model. Compos Part B: Engng, 42 (6) (2011), pp. 1539-1553.
6. F. Ceroni, M. Pecce, A. Bilotta, E. Nigro. Bond behavior of FRP NSM systems in concrete elements. Compos Part B: Engng, 43 (2) (2012), pp. 99-109.
7. J. Yao, J. Teng, J. Chen, Experimental study on FRP-to-concrete bonded joints Composites: Part B, 36 (2005), pp. 99–113.
8. L. De Lorenzis, J. Teng. Near-surface mounted FRP reinforcement: an emerging technique for strengthening structures. J Compos, Part B, 38 (2007), pp. 119–43.
9. F. Ceroni, M. Pecce, S. Matthys, L. Taerwe. Debonding strength and anchorage devices for reinforced concrete elements strengthened with FRP sheets. Composites: Part B, 39 (3) (2008), pp. 429-441.
10. H. Rasheed, K. Larson, R. Peterman. Analysis and design procedure for FRP-strengthened prestressed concrete T-Girders considering strength and fatigue. J. Compos. for Constr., ASCE, 10 (5) (2006), pp. 419-432.
11. C. Mazzoti, M. Savoia, B. Ferracuti. An experimental study on delamination of FRP plates bonded to concrete. Constr. Build. Mater., 22 (7) (2008), pp. 1409-1421.

12. X. Chang, Q. Wang, P. Zhang. Modeling of single-flexural crack induced debonding of FRP plate strengthened concrete beams based on an assumption of heterogeneity. Composites: Part B, 43 (3) (2012), pp. 1598-1603.

13. T. El-Maaddawy, S. Sherif. FRP composites for shear strengthening of reinforced concrete deep beams with openings. Journal of Composite Structures, 60 (2009), pp. 197–204.

14. C. Zhang, J. Wang. Interface stress redistribution in FRP-strengthened reinforced concrete beams using a three-parameter viscoelastic foundation model. Composites: Part B, 2012, In Press.

15. K. Al-Tamimi, R. Hawileh, J. Abdalla, H. Rasheed. Effects of Ratio of CFRP Plate Length to Shear Span and End Anchorage on Flexural Behavior of SCC R/C Beams. J. Compos. for Constr. ASCE, 2011, 15 (6), pp. 875-1002.

16. American Concrete Institute Technical Committee440. Guide for the design and construction of externally bonded FRP systems for strengthening concrete structures. ACI 440.2R-08, 2008.

17. O. Rosenboom, S. Rizkalla. Experimental Study of Intermediate Crack Debonding in Fiber-Reinforced Polymer Strengthened Beams. ACI Structural Journal, 105 (1) (2008), pp. 41-50.

18. P. Whitehead, T. Ibell. Novel Shear Reinforcement for Fiber-Reinforced Polymer-Reinforced and Prestressed Concrete. ACI Structural Journal, 102 (5) (2005), pp. 286-294.

19. X. Lu, L. Ye, J. Teng, J. Jiang. Meso-scale finite element model for FRP sheets/plates bonded to concrete. Engineering Structures, 27 (4) (2005), pp. 564-575.

20. R. Hawileh. Nonlinear finite element modeling of RC beams strengthened with NSM FRP rods, Construction and Building Materials, 27 (2011), pp. 461–471.

21. R. Hawileh, T. El-Maaddawy, M. Naser. Non-linear Finite Element Modeling of Concrete Deep Beams with Openings Strengthened with Externally-Bonded Composites. Materials and Design, Elsevier, (2012), Accepted.

22. G. Chen, J. Chen, J. Teng. On the finite element modelling of RC beams shear-strengthened with FRP. Construction and Building Materials, 32 (1) (2012), pp. 13-26.

23. ANSYS. ANSYS workbench documentation. Version 11. Canonsburg (PA): ANSYS Inc.; 2007.

24. R. Hawileh, J. Abdalla, M. Tanarslan, M. Naser. Modeling of Nonlinear Cyclic Response of Shear-Deficient RC T-beams strengthened with Side Bonded CFRP Fabric Strips. Computers and Concrete, An Int'l Journal 8 (12) (2011), pp. 193-206.

25. E. Hognestad, N. Hanson, D. McHenry. Concrete stress distribution in ultimate strength design. ACI Journal, Proceedings, 52 (12) (1955), pp. 455–479.

26. Comite Euro-International du Beton (CEB-FIP). CEB-FIP model code 1990. Bulletin D'Information No. 213/214 (Concrete Structures), Lausanne, Switzerland; 1993.

27. J. Nie, J. Fan, C. Cai. Stiffness and deflection of steel–concrete composite beams under negative bending. J Struct Eng., 130 (11) (2004), pp. 1842-1851

28. X. Xu, A. Needleman. Numerical simulations of fast crack growth in brittle solids. J Mech Phys Solids, 42 (1994), pp. 1397–1434

Please cite this paper as:
Rami A. Hawileh, Mohannad Z. Naser, Jamal A. Abdalla, Finite element simulation of reinforced concrete beams externally strengthened with short-length CFRP plates, Composites Part B: Engineering, Volume 45, Issue 1, February 2013, Pages 1722-1730, ISSN 1359-8368, https://doi.org/10.1016/j.compositesb.2012.09.032.

29. K. Nakaba, T. Kanakubo, T. Furuta, H. Yoshizawa. Bond behavior between fiber reinforced polymer laminates and concrete. ACI Structural Journal, 98 (3) (1998), pp. 359-367.

30. R. Hawileh, J. Abdalla, M. Tanarslan. Modeling of Nonlinear Response of R/C Shear Deficient T-Beam Subjected to Cyclic Loading. Computers and Concrete, An Int'l Journal 2012, In Press.

List of Figures

Fig. 1. Details of tested beams and location of two point loadings [15]

Fig. 2. Details of the developed FE model

Fig. 3. Load-midspan deflection response for the CB and B90P specimens

Fig. 4. Load-midspan deflection response for the B50P and B50PW specimens

Fig. 5. Load-midspan deflection response for the B05WD and B50PW1 specimens

Fig. 6. Comparison between the failure modes of the experimental and FE models

Fig. 7. Effect of bar size on the performance of B50P specimens

Please cite this paper as:
Rami A. Hawileh, Mohannad Z. Naser, Jamal A. Abdalla, Finite element simulation of reinforced concrete beams externally strengthened with short-length CFRP plates, Composites Part B: Engineering, Volume 45, Issue 1, February 2013, Pages 1722-1730, ISSN 1359-8368, https://doi.org/10.1016/j.compositesb.2012.09.032.

Fig. 8. Effect of bar size on the performance of B50PW specimens

Fig. 9. Effect of bar size on the performance of B50PW1 specimens

Fig. 10. Effect of bar size on the performance of B50PWD specimens

Fig. 11. Comparison of between FE-B50PW1, FE-B50PWD and FE-B50PWD1

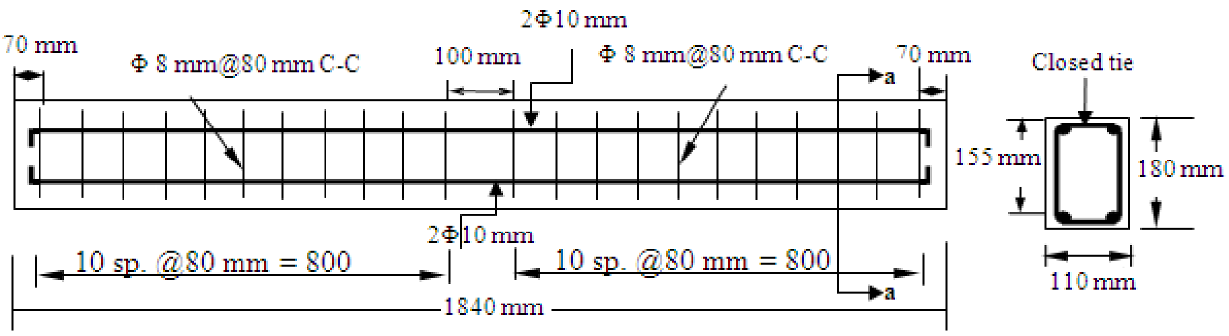

(a) Longitudinal and cross-section reinforcement details of the beam

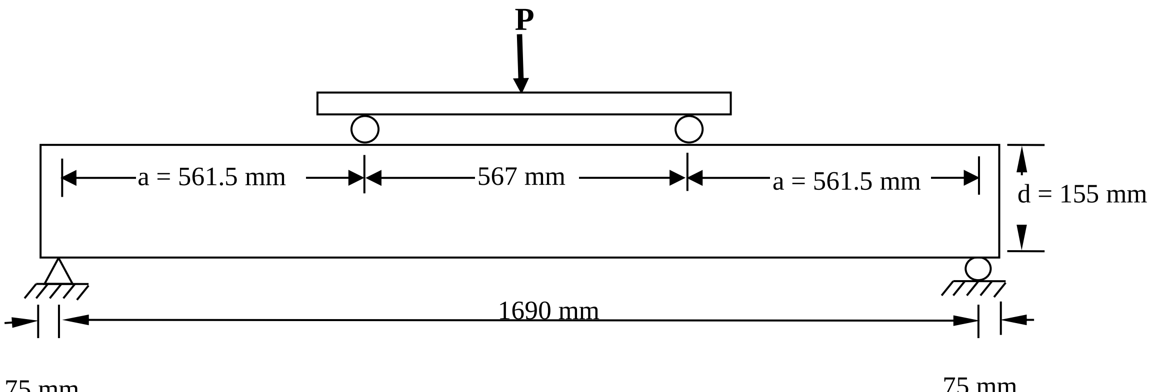

(b) Tested beam details and location of two point loadings

Fig. 1. Details of tested beams and location of two point loadings [15]

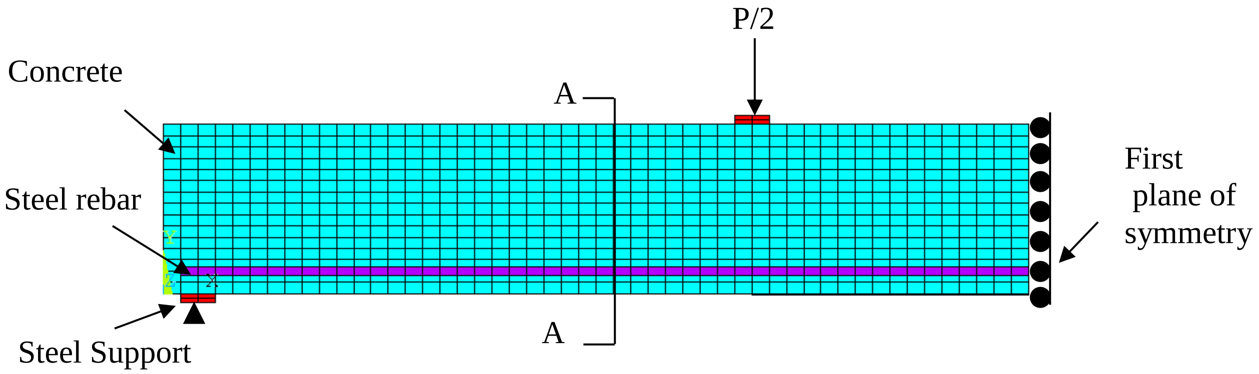

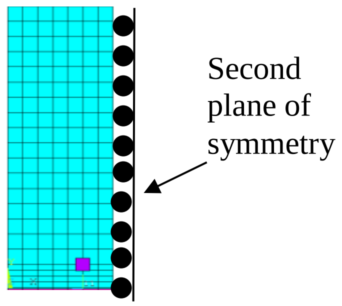

Section A-A

(a) FE-CB

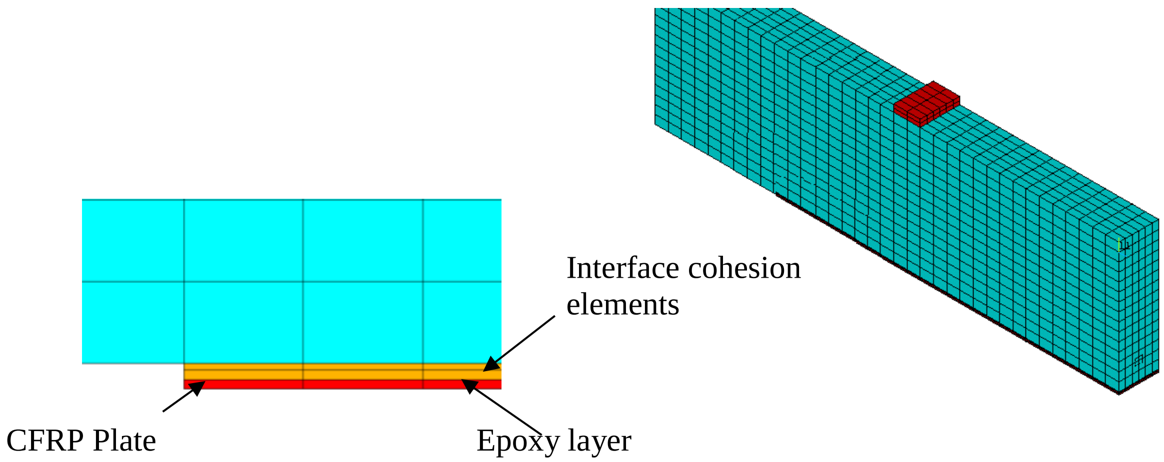

(b) FE-B50P

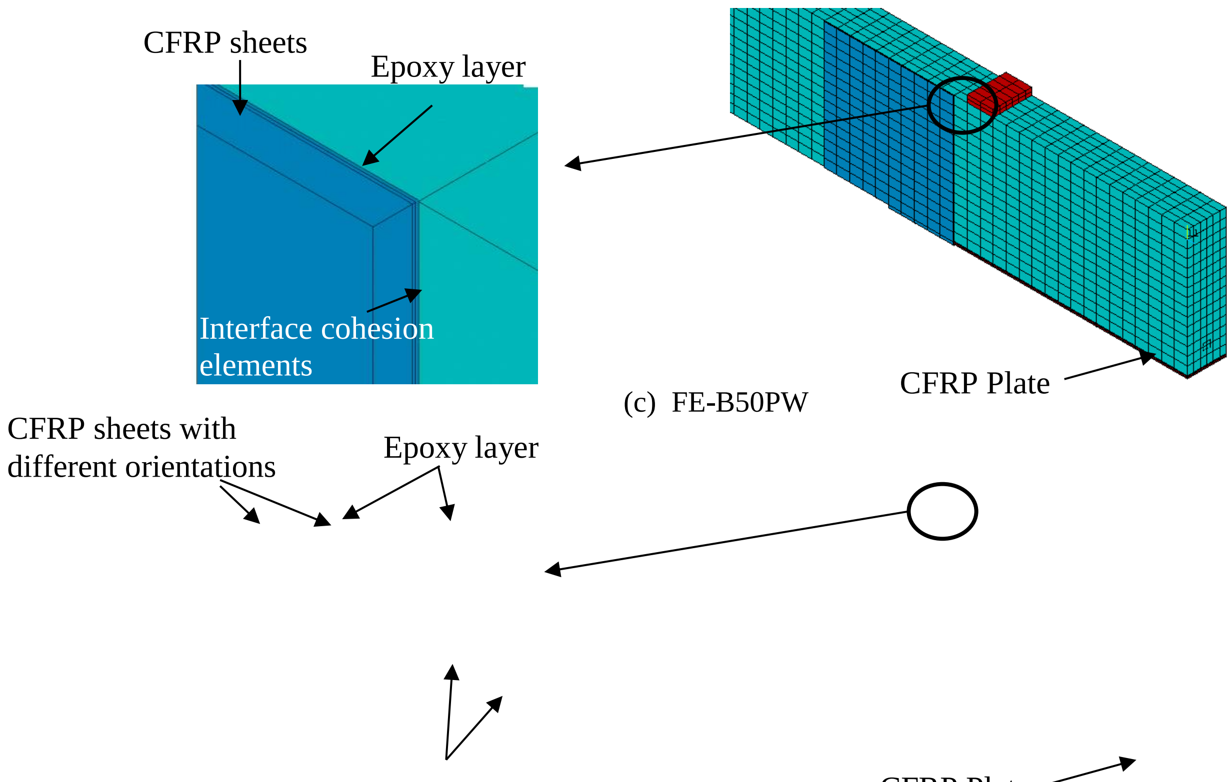

(c) FE-B50PW

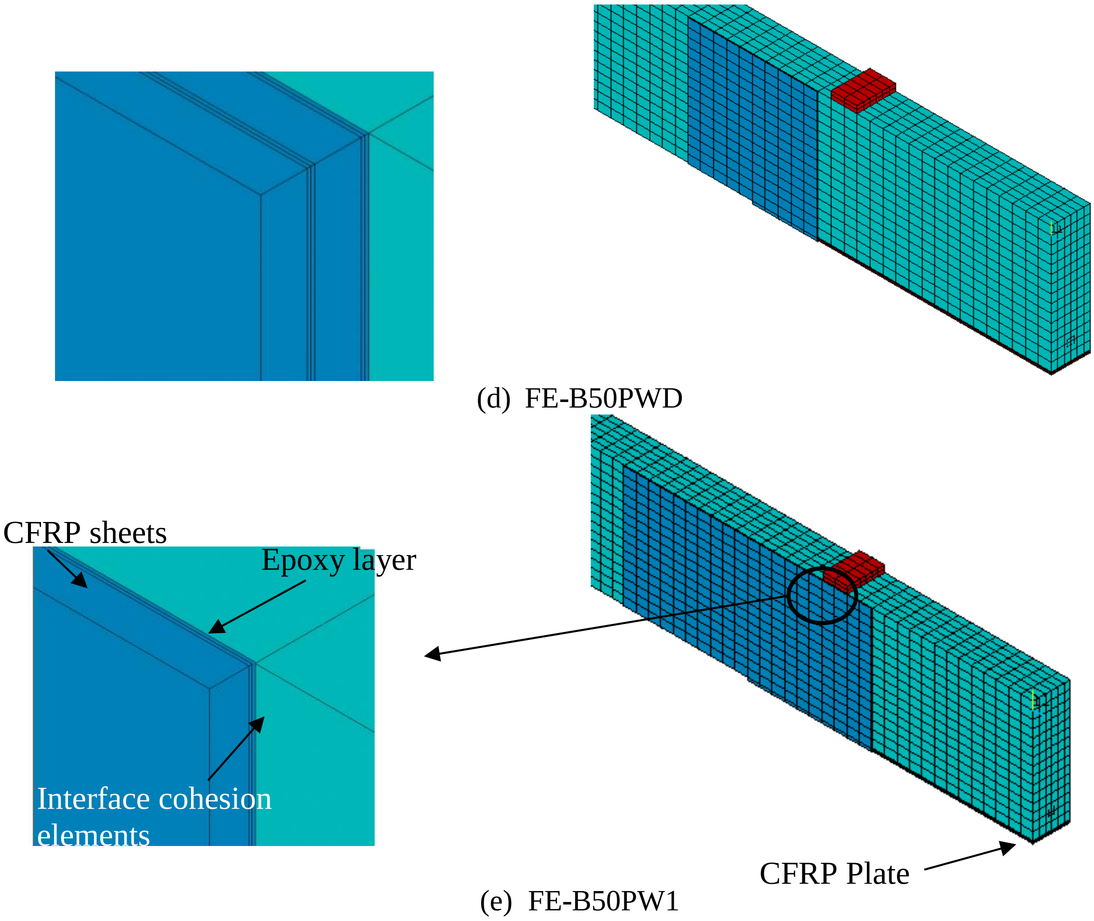

Fig. 2. Details of the developed FE model

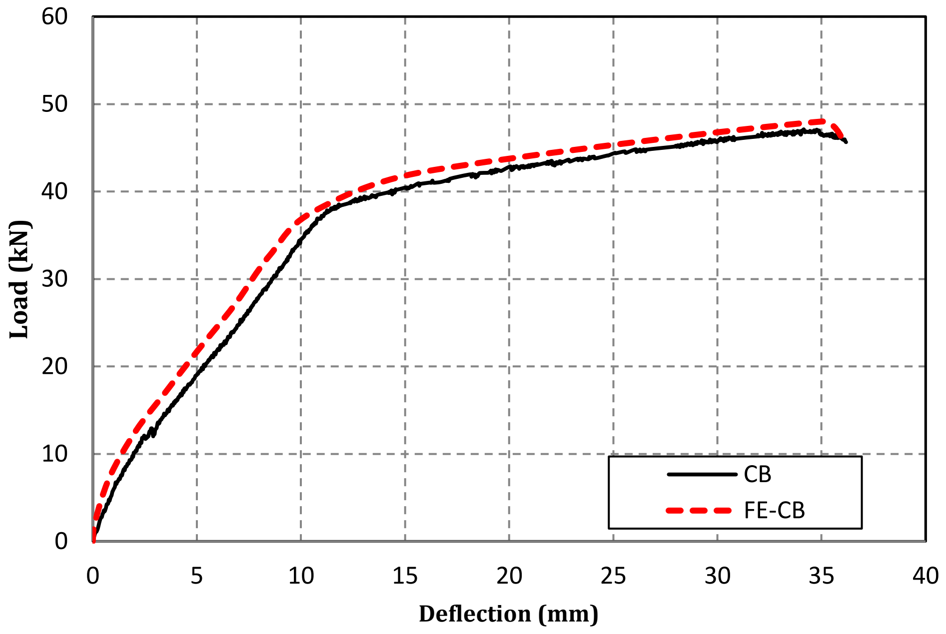

(a) CB

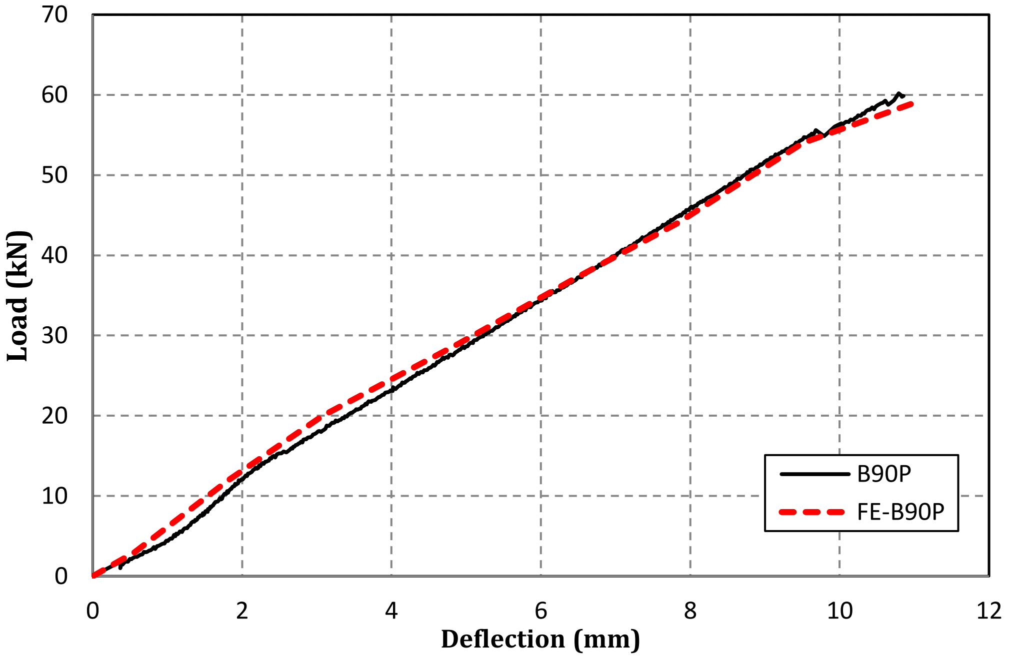

(b) B90P

Fig. 3. Load-midspan deflection response for the CB and B90P specimens

This is a preprint draft. The published article can be found at:
http://www.sciencedirect.com/science/article/pii/S135983681200580X

Please cite this paper as:
Rami A. Hawileh, Mohannad Z. Naser, Jamal A. Abdalla, Finite element simulation of reinforced concrete beams externally strengthened with short-length CFRP plates, Composites Part B: Engineering, Volume 45, Issue 1, February 2013, Pages 1722-1730, ISSN 1359-8368, https://doi.org/10.1016/j.compositesb.2012.09.032.

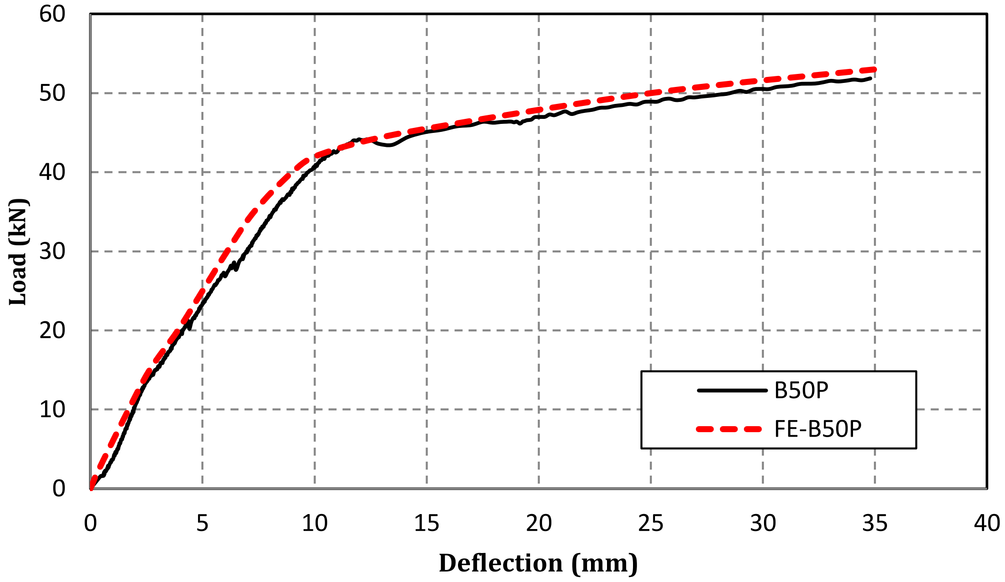

(c) B50P

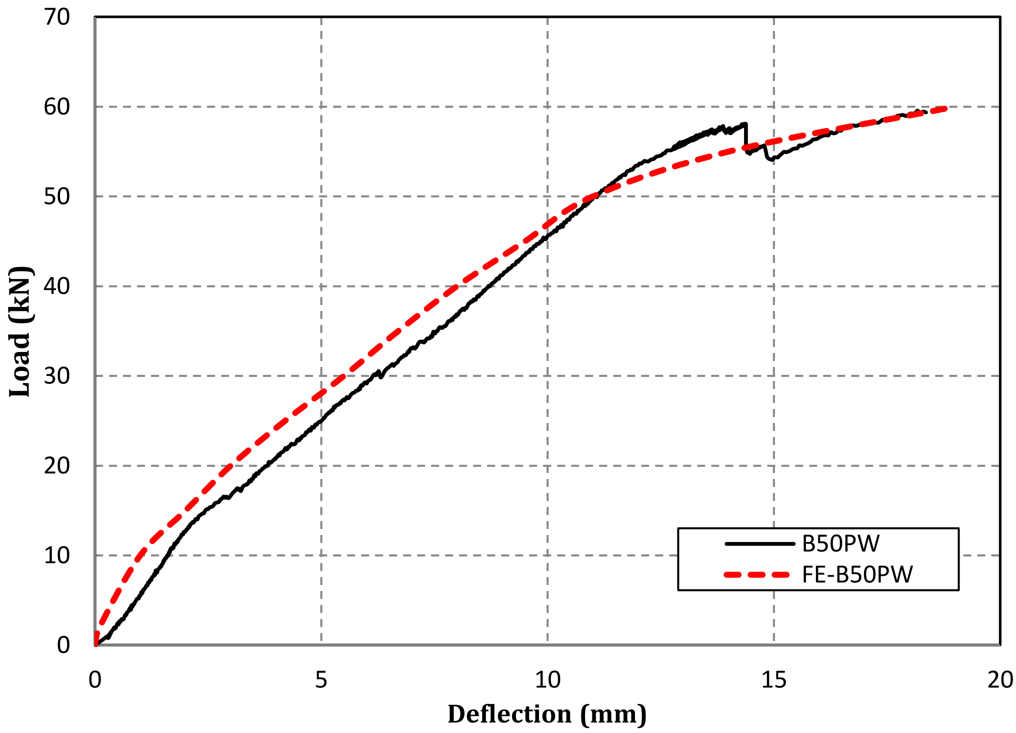

(d) B50PW

Fig. 4. Load-midspan deflection response for the B50P and B50PW specimens

This is a preprint draft. The published article can be found at:
http://www.sciencedirect.com/science/article/pii/S135983681200580X

Please cite this paper as:
Rami A. Hawileh, Mohannad Z. Naser, Jamal A. Abdalla, Finite element simulation of reinforced concrete beams externally strengthened with short-length CFRP plates, Composites Part B: Engineering, Volume 45, Issue 1, February 2013, Pages 1722-1730, ISSN 1359-8368, https://doi.org/10.1016/j.compositesb.2012.09.032.

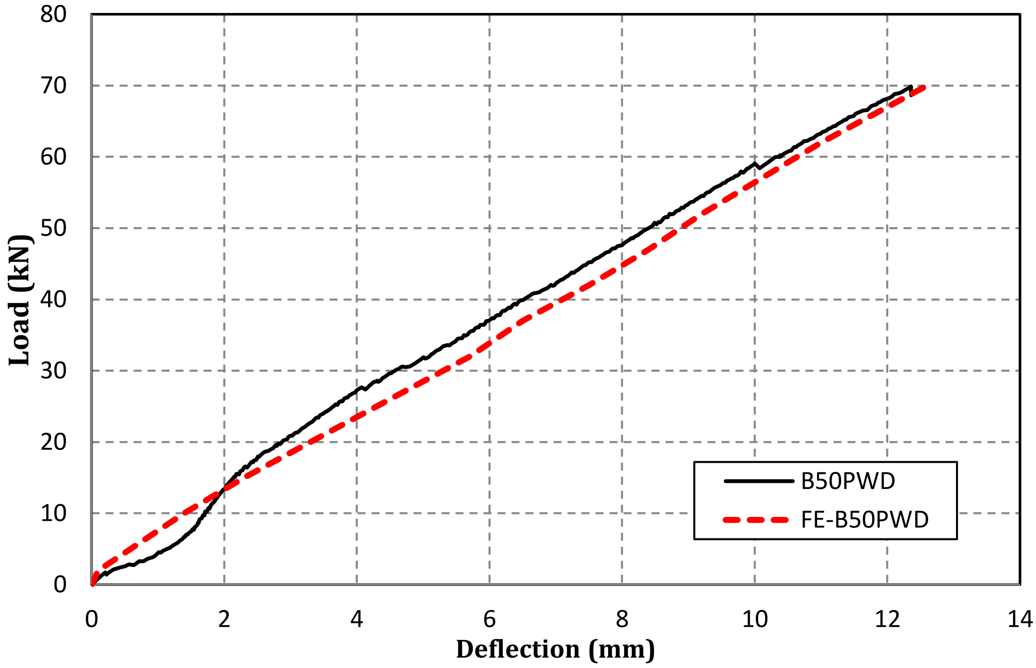

(a) B50PWD

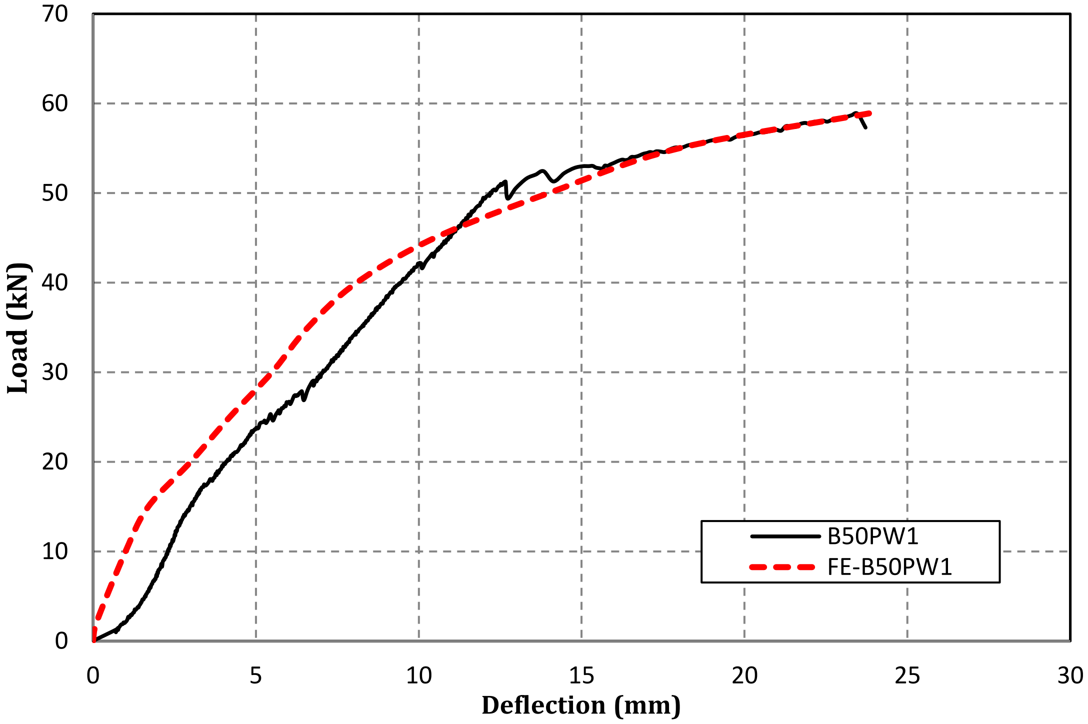

(b) B50PW1

This is a preprint draft. The published article can be found at:
http://www.sciencedirect.com/science/article/pii/S135983681200580X

Please cite this paper as:
Rami A. Hawileh, Mohannad Z. Naser, Jamal A. Abdalla, Finite element simulation of reinforced concrete beams externally strengthened with short-length CFRP plates, Composites Part B: Engineering, Volume 45, Issue 1, February 2013, Pages 1722-1730, ISSN 1359-8368, https://doi.org/10.1016/j.compositesb.2012.09.032.

Fig. 5. Load-midspan deflection response for the B05WD and B50PW1 specimens

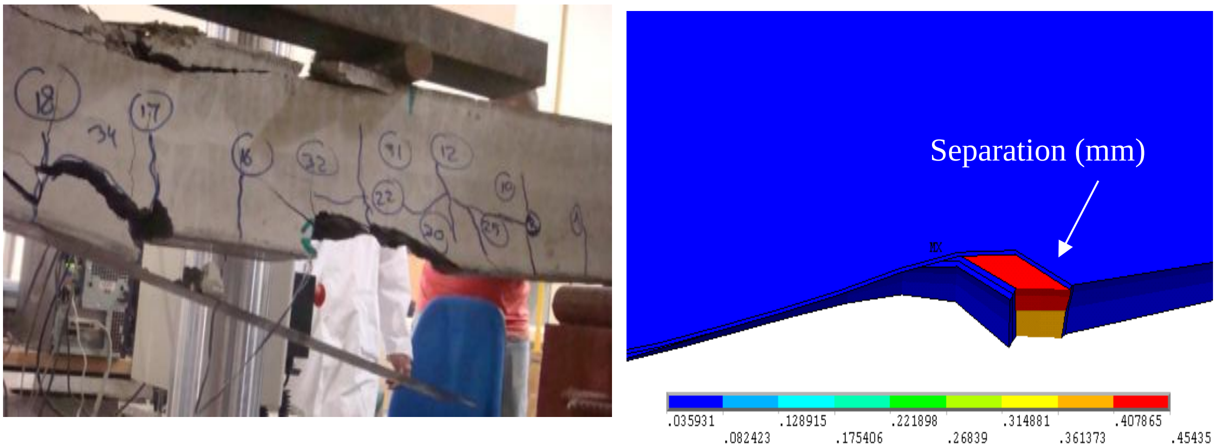

(a) CFRP plate de-bonding of B50P and FE- B50P

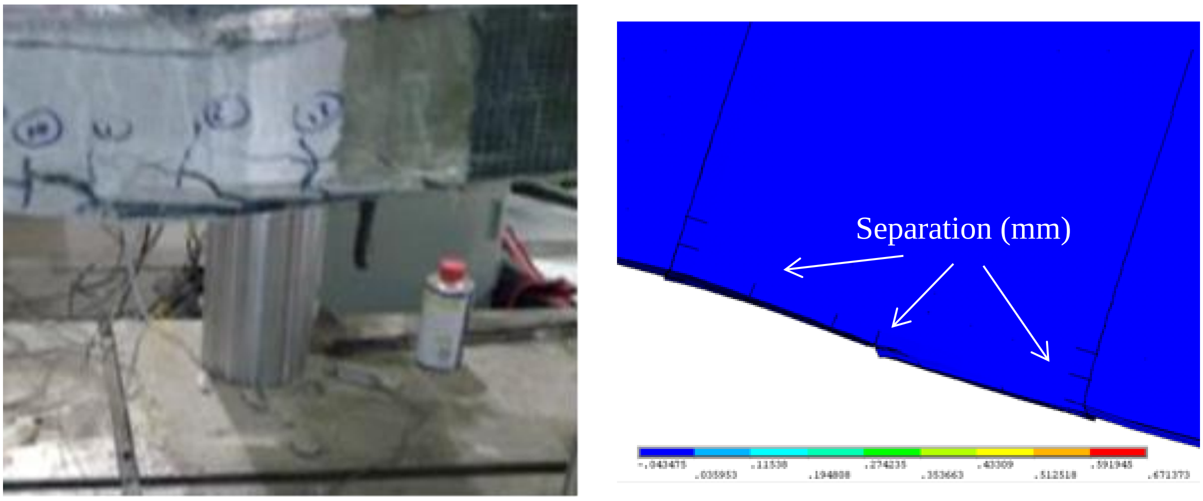

(b) Cover delamination of B50PW and FE- B50PW

Fig. 6. Comparison between the failure modes of the experimental and FE models

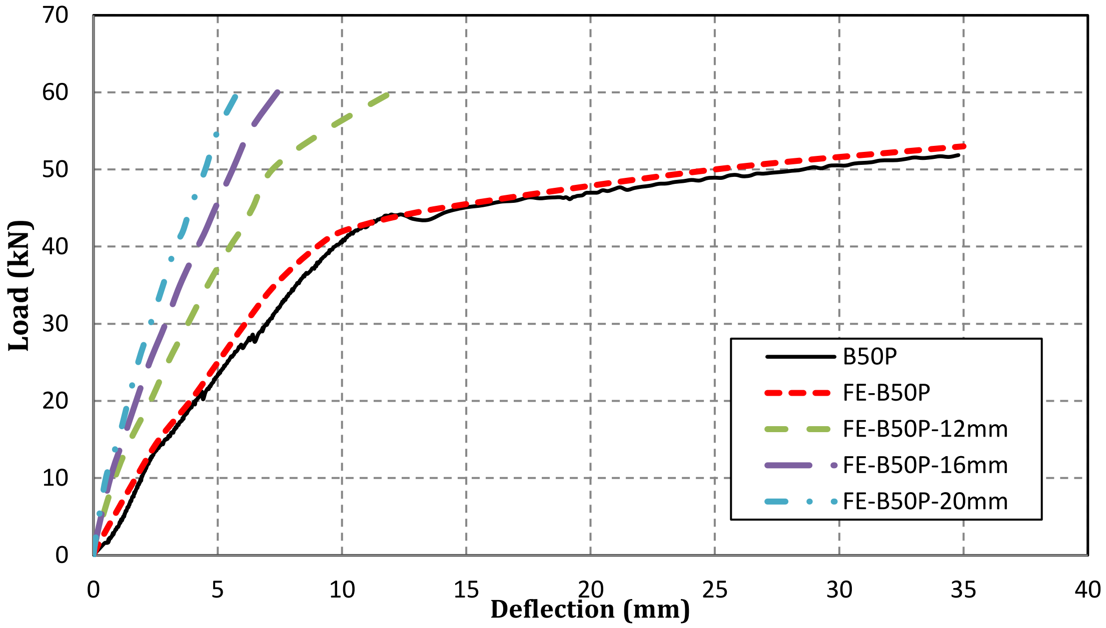

Fig. 7. Effect of bar size on the performance of B50P specimens

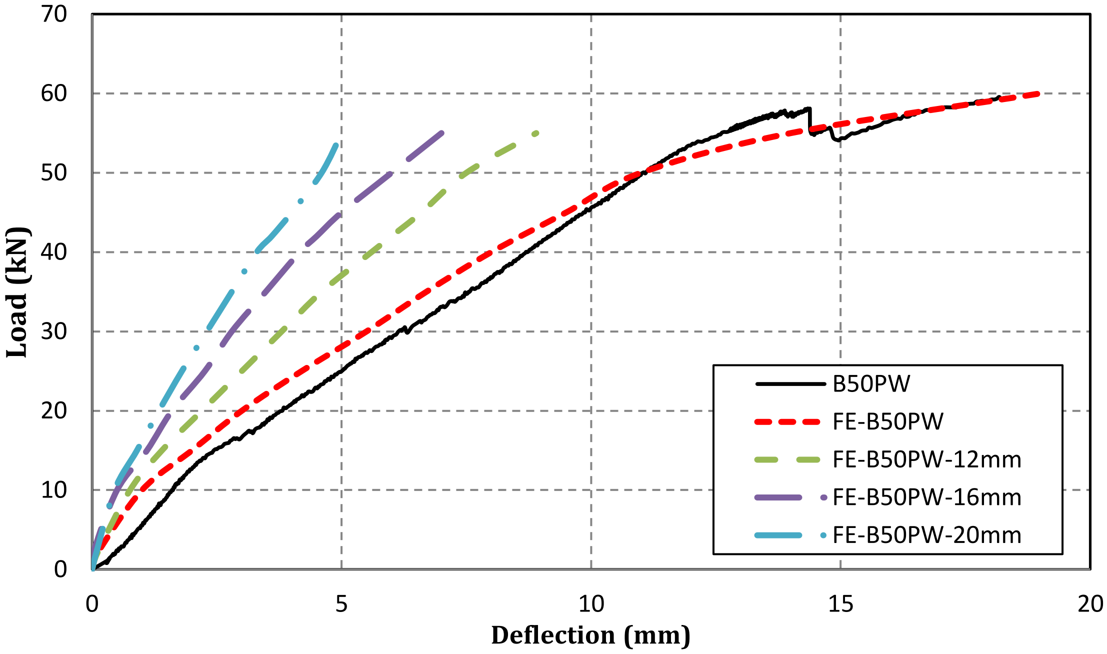

Fig. 8. Effect of bar size on the performance of B50PW specimens

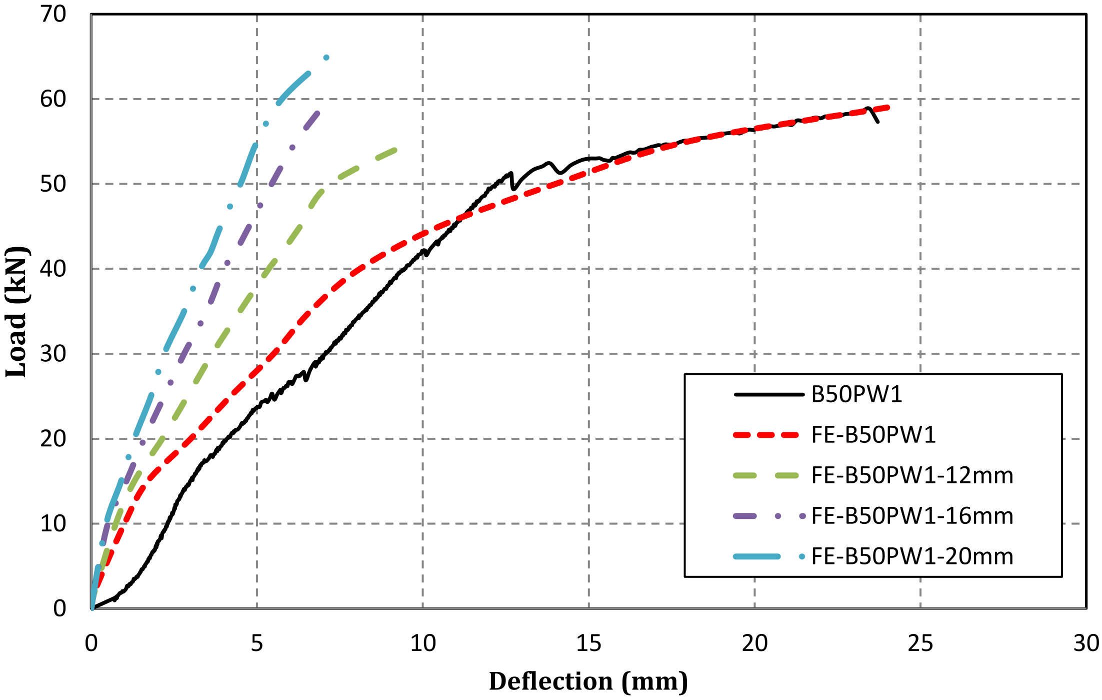

Fig. 9. Effect of bar size on the performance of B50PW1 specimens

This is a preprint draft. The published article can be found at:
http://www.sciencedirect.com/science/article/pii/S135983681200580X

Please cite this paper as:
Rami A. Hawileh, Mohannad Z. Naser, Jamal A. Abdalla, Finite element simulation of reinforced concrete beams externally strengthened with short-length CFRP plates, Composites Part B: Engineering, Volume 45, Issue 1, February 2013, Pages 1722-1730, ISSN 1359-8368, https://doi.org/10.1016/j.compositesb.2012.09.032.

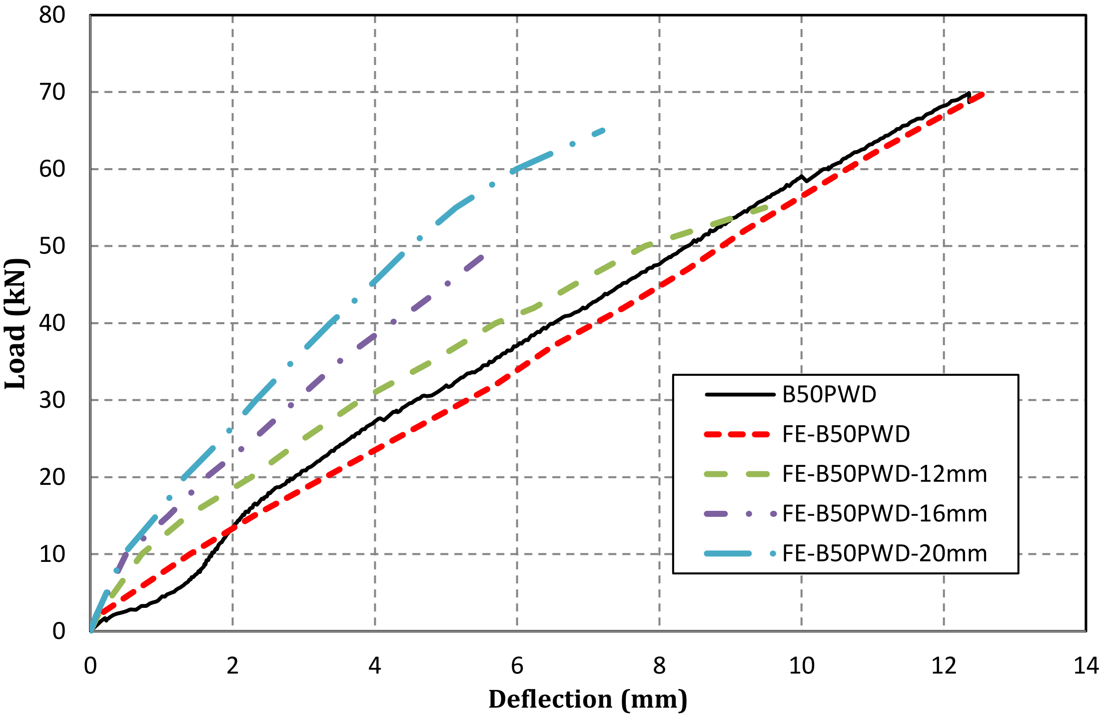

Fig. 10. Effect of bar size on the performance of B50PWD specimens

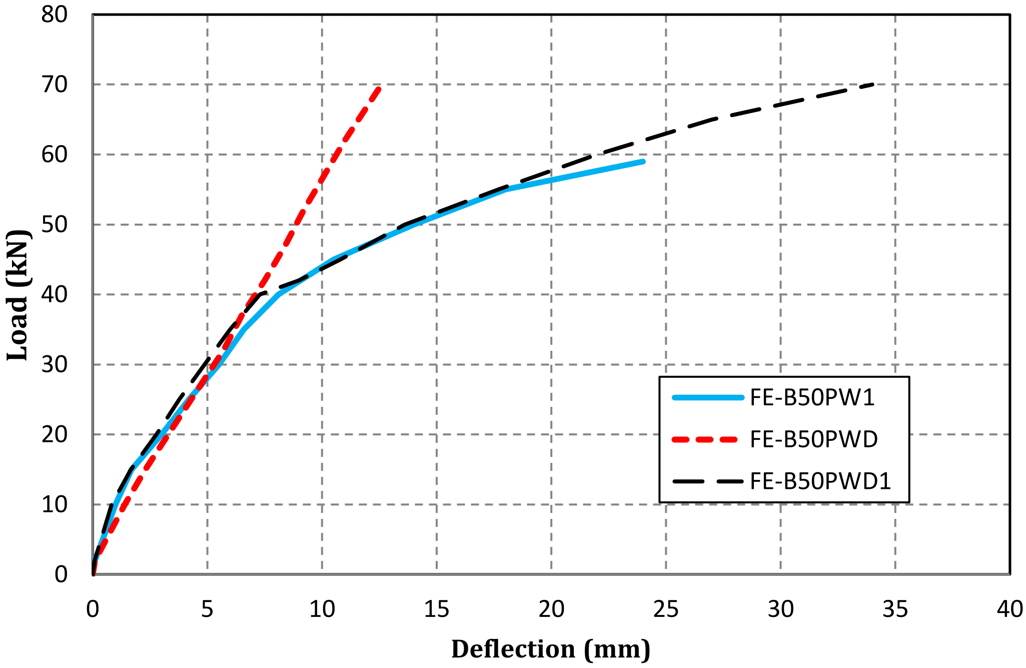

Fig. 11. Comparison of between FE-B50PW1, FE-B50PWD and FE-B50PWD1

Please cite this paper as:
Rami A. Hawileh, Mohannad Z. Naser, Jamal A. Abdalla, Finite element simulation of reinforced concrete beams externally strengthened with short-length CFRP plates, Composites Part B: Engineering, Volume 45, Issue 1, February 2013, Pages 1722-1730, ISSN 1359-8368, https://doi.org/10.1016/j.compositesb.2012.09.032.

List of Tables:

Table 1.Experimental and numerical matrix used

Table 2. Model Validation

Table 3. Effect of varying bar size of the steel tensile reinforcement

Table 1.Experimental and numerical matrix used

Specimen	FE Model	Length of CFRP Plate (mm)	Shear Span length of CFRP (%)	Width of CFRP U-wrap sheet(mm)
CB	FE-CB	0	0	0
B90P	FE-B90P	1521	85	0
B50P	FE-B50P	845	25	0
B50PW	FE-B50PW	845	25	200
B50PW1	FE-B50PW1	845	25	400
B50PWD	FE-B50PWD	845	25	200×2 (2 directions)

Table 2. Model Validation

Specimen	**FE Model**	**Ultimate Load (kN)**		**Difference %**	**Ultimate Deflection (mm)**		**Difference %**
		Exp.	FE	1-(Exp./FE)	Exp.	FE	1-(Exp./FE)
CB	FE-CB	47.7	48.0	0.6%	35.7	36.0	0.8%
B90P	FE-B90P	60.2	59.1	-1.9%	10.8	11.2	3.6%
B50P	FE-B50P	51.9	53.2	2.4%	34.6	34.8	0.6%
B50PW	FE-B50PW	59.56	60.1	0.9%	18.5	19.0	2.6%
B50PW1	FE-B50PW1	58.88	59.4	0.9%	24.4	25.0	2.4%
B50PWD	FE-B50PWD	68.66	70.0	1.9%	12.1	12.5	3.2%

This is a preprint draft. The published article can be found at:
http://www.sciencedirect.com/science/article/pii/S135983681200580X

Please cite this paper as:
Rami A. Hawileh, Mohannad Z. Naser, Jamal A. Abdalla, Finite element simulation of reinforced concrete beams externally strengthened with short-length CFRP plates, Composites Part B: Engineering, Volume 45, Issue 1, February 2013, Pages 1722-1730, ISSN 1359-8368, https://doi.org/10.1016/j.compositesb.2012.09.032.

Table 3. Effect of varying bar size of the steel tensile reinforcement

FE Model	Failure Load (kN)	Increase over validated model (%)	Maximum Deflection (mm)	Decrease over validated model (%)	Failure Mode
FE-B50P	*51.9*	-	*34.6*	-	Steel yielding and Debonding
FE-B50P-12mm	57	9.8	12	65.3	Steel yielding, Debonding and Concrete crushing
FE-B50P-16mm	59	13.7	7.4	78.6	Debonding
FE-B50P-20mm	60	15.6	5.8	83.2	Debonding
FE-B50PW	*59.56*	-	*18.5*	-	Concrete cover delamination
FE-B50PW-12mm	52	-12.7	12	35.1	Steel yielding, Debonding and minor Concrete crushing
FE-B50PW-16mm	55	-7.7	7.4	60.0	Debonding
FE-B50PW-20mm	53	-11.0	5.8	68.6	Debonding
FE-B50PW1	*58.88*	--	10	-	Steel yielding and Debonding
FE-B50PW1-12mm	55	-6.6	12	-50.8	Steel yielding and Debonding
FE-B50PW1-16mm	75	27.4	7.4	69.7	Steel yielding and Debonding
FE-B50PW1-20mm	65	10.4	5.8	76.2	Debonding

FE-B50PWD	68.66	-	10	-	Steel yielding, Debonding and Concrete crushing
FE-B50PWD-12mm	60	-12.6	12	-0.8	Steel yielding, Debonding and Concrete crushing
FE-B50PWD-16mm	50	-27.2	7.4	38.8	Steel yielding and Debonding
FE-B50PWD-20mm	65	-5.3	5.8	52.1	Steel yielding and Debonding